Tuning the Band Alignment and Electronic Properties of GaSe/SnX_2 (X = S, Se) Two-Dimensional van der Waals Heterojunctions via an Electric Field

Bo Sun,[1] Yu-Feng Ding,[1] Peng-Bin He,[1,*] Yu-Qing Zhao,[2] and Meng-Qiu Cai[1,†]

[1] *Key Laboratory for Micro/Nano Optoelectronic Devices of Ministry of Education & Hunan Provincial Key Laboratory of Low-Dimensional Structural Physics and Devices, School of Physics and Electronics, Hunan University, Changsha 410082, China*

[2] *School of Physics and Electronic Science, Hunan University of Science and Technology, Xiangtan 411201, People's Republic of China*

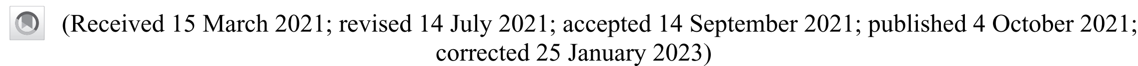

(Received 15 March 2021; revised 14 July 2021; accepted 14 September 2021; published 4 October 2021; corrected 25 January 2023)

Two-dimensional (2D) material-based van der Waals heterostructures (vdWHs) have been identified as an excellent platform from which to expand various device applications for light-emitting, photovoltaic, and field-effect transistors because of their different band alignments, including type-I, type-II, and type-III. However, it is difficult to achieve transformations between types of band alignment in a single heterostructure for diverse applications. In this study, the effects of a vertical electric field on the band alignment transition and electronic properties of 2D GaSe/SnS_2 ($SnSe_2$) vdWHs are investigated systematically using density functional theory calculations. The study shows that the electric field can modulate not only the band gap but also the band alignment to produce multifunctional device applications. A positive electric field can control the band alignment transformation from type-II to type-I for electric field values of approximately 0.39 V/Å (0.12 V/Å), while a negative electric field can transform the type-II to type-III band alignments for electric field values of about −0.2 V/Å (−0.16 V/Å) in GaSe/SnS_2 ($SnSe_2$) vdWHs. We trace these surprising results to the conduction band and valence band edge position movements for the linear decrease of GaSe, while the linear increase of SnS_2 ($SnSe_2$) occurs with the applied electric field. The present work may provide a direction for tunable multiple-band alignments in 2D vdWHs and help achieve multifunctional device applications.

DOI: 10.1103/PhysRevApplied.16.044003

I. INTRODUCTION

Two-dimensional (2D) materials have been widely used in various fields owing to their excellent electronic, mechanical, and optical properties [1–6]. Nevertheless, single ultra-thin 2D nanomaterials cannot meet the increasing application requirements in various fields. The lack of band gaps in graphene, for instance, reduces its range of applications in high-speed nanodevices [7]. The relatively low electronic mobility of MoS_2 restricts its development and application [8]. As a result, scientists have been forced to expand into promising areas. Some studies have shown that the construction of van der Waals heterostructures (vdWHs), in which one 2D material is stacked on another, is a good way to expand the application field of 2D materials. This method can not only integrate the advantages of various 2D materials, as well as expand and modify the properties of a single 2D material, but also show excellent properties that a single material does not have [6,9–13]. For example, the van der Waals interfaces of tungsten selenide and black phosphorus designed by Akamatsu *et al.* produce in-plane polarization and spontaneous photovoltaic effects [14]. In addition, when different materials are in contact, the vdWHs will form three different band alignments, including straddling type-I, staggered type-II, and broken-gap type-III, which can be applied in various fields [15,16]. The type-I vdWHs can be used in light-emitting device applications, such as light-emitting diodes (LEDs) [17,18]. The type-II vdWHs have great potential in the field of high-performance photovoltaic devices and the photocatalytic decomposition of water [19,20]. The type-III vdWHs play an important role in tunneling field-effect transistors (TFETs) [6,21,22].

Although the application of heterostructures with different band types in various fields has been significantly developed, it is still difficult to adopt heterostructures with only one specific band alignment for different applications. Therefore, in order to design a flexible, multifunctional application device based on vdWHs, it is essential to have dynamic modulation of band alignments. It has been reported that the band alignment and electronic properties of heterojunctions can be effectively tuned by doping, using external stress, applying an electric field, and

*hepengbin@hnu.edu.cn
†mqcai@hnu.edu.cn

 © 2021 American Physical Society

changing the interlayer distance [8,23,24]. For example, Shehzad *et al.* found that WTe_2/As heterostructures showed a type-I to type-II transition of the band alignment for an appropriate compressive strain of 2% and 3%, which could slow down electron-hole pair recombination [25]. Lin *et al.* found that I-ion doping could transform a type-I BiOCl/BiOBr structure into a type-II I-BiOCl/I-BiOBr system, acquiring more favorable visible light absorption [26]. Chen *et al.* found that the band alignment transition from type-I to type-II in $InSe/MoS_2$ vdWHs could be controlled by changing the interlayer separation [27]. However, it should be pointed out that it is not easy to regulate 2D materials by means of stress (the low strain efficiency), ion doping (difficulty in operation), and interlayer regulation (complexity of the device fabrication process). Nevertheless, applying a vertical electric field is a more feasible means of controlling heterojunctions, and this control method is also expected to be dynamic, reversible, and free from impurities. Zhou *et al.* found that an external electric field could be applied to control the band alignment of In_2Se_3/MoS_2 vdWHs from type-II to type-I when the electric field value was 0.6 V/Å, making the method suitable for luminescent device applications [28].

In recent years, a kind of heterostructure composed of group-III monochalcogenides (*MX, M* = Ga, In; *X* = S, Se.) has shown great application potential in optoelectronics [29–31]. It has been reported that a 2D monochalcogenide GaSe monolayer has been successfully produced with a mechanical exfoliation technique [32] or vapor phase deposition approach [33]. A GaSe monolayer consists of strong covalent bonds in a series of Se—Ga—Ga—Se [34,35]. In addition, owing to its intriguing properties, such as the thermal stability, high photoresponsivity of 1.7 A/W at zero gate voltage, and anisotropic Hall-mobility of about $215\,cm^2\,V^{-1}\,s^{-1}$, a GaSe monolayer has a wide range of applications in transistors, photocatalysts, solar cells, and other fields [36]. Compared with other 2D monochalcogenides, such as InSe and GaTe, GaSe is known for its nonlinear optics, and can be combined with different layered materials, such as transition metal disulfides (TMDs) to create attractive functions [37]. Typical TMD compounds SnS_2 and $SnSe_2$ belonging to the sandwich configuration consisting of covalent bonds S—Sn—S and Se—Sn—Se have attracted much attention [38]. Moreover, due to their excellent photoelectric properties, including a high on:off ratio ($>10^6$), light response ($>106\,A\,W^{-1}$), and carrier mobility ($>230\,cm^2\,V^{-1}\,s^{-1}$), SnS_2 and $SnSe_2$ have been applied in the fields of photodetectors, photoelectronic nanodevices, field-effect transistors, and so on [39,40]. Compared with graphene, MX_2 exhibits better electronic and optical properties in an external electric field due to its appropriate band gap.

Interestingly, combining semiconductor *MX* materials with MX_2 can integrate the excellent optical properties of these materials, and this combination promises to produce materials for highly responsive photodetectors [41,42]. Perumal *et al.* have experimentally synthesized $GaSe/SnS_2$ heterojunctions, which have been used in phototransistors, photovoltaic cells, and photodetectors [42]. The study showed that the $GaSe/SnS_2$ vdWHs possessed type-II band alignment with an indirect band gap, which could significantly improve the efficiency of the electron-hole pair separation, but the physical mechanisms of the band alignment were still unclear. Therefore, we present a detailed theoretical study not only of the physical mechanisms of the band alignment of stacked 2D $GaSe/SnX_2$ ($X =$ S, Se) vdWHs, but also of the effects of a vertical electric field on band alignment transition and electronic properties, using density functional theory (DFT) calculations to further expand the application of the heterojunctions in various fields. The results show that the $GaSe/SnS_2$ ($SnSe_2$) vdWHs possess type-II band alignment and the band gap is significantly reduced compared to each 2D component of the vdWH. Moreover, the type-I and type-III band alignments are also created in an external electric field, suggesting their potential applications in multifunctional nanoelectronic and optoelectronic devices.

II. COMPUTATIONAL METHODS

In this study, the DFT calculations are implemented in the Vienna *ab initio* simulation package, in which the projector-augmented wave method is used to simulate the electron-ion potential [41–46]. The Perdew-Burke-Ernzerhof (PBE) function of the generalized gradient approximation with the DFT-D3 correction method of Grimme *et al.* is used to describe the exchange and correlation effects [47–54]. To avoid periodic interaction between the adjacent layers, the thickness of the vacuum space in the *z* direction is set to 20 Å. A gamma-centered *k*-point grid of $5 \times 5 \times 1$ using the Monkhorst-Pack scheme and a 400 eV plane-wave basis cutoff are applied to produce the structural optimizations and self-consistency in the first Brillouin zone of the GaSe and SnX_2 monolayers and their heterostructures. To find the fully relaxed structures, the total energy and all forces on the atoms must be less than 10^{-5} eV and 0.01 eV/Å, respectively. The high symmetry points of the first Brillouin region in the energy band structure are taken as *G* (0 0 0), *M* (0 0.5 0), and *K* (−0.33 0.66 0). In addition, we use the Heyd-Scuseria-Ernzerhof (HSE06) hybrid function to calculate the electronic band structure in order to partially compensate for the underestimation of the band gap by the semilocal function [55]. However, the PBE method is more convenient than the HSE method for calculating almost the same band trend of the electronic properties in the heterojunctions in the external electric field due to the low cost. Thus, the intrinsic electronic properties of the 2D $GaSe/SnS_2$ ($SnSe_2$) vdWHs and the corresponding isolated monolayers are

calculated with the HSE06 method to correct the underestimated band gaps, while the variation trend of the electronic properties in an applied external electric field is determined by the PBE method. The HSE method is used to correct the band gap and edge values, for which a percentage (25%) of the exact nonlocal Hartree-Fock exchange is added to the PBE function to correct the gap values and the band edges [56]. In addition, the spin-orbit coupling effect has no significant effect on the 2D materials. All images are created with VESTA and ORIGIN.

III. RESULTS AND DISCUSSION

A. Geometric structure of GaSe/SnS_2 ($SnSe_2$) vdWHs

Figure 1 shows the (a) top view and (b) side view of the relaxed geometric structure of the GaSe/SnS_2 ($SnSe_2$) vdWHs. The GaSe/SnS_2 ($SnSe_2$) vdWHs are formed by the superposition of single cells GaSe and SnS_2 ($SnSe_2$) along the c direction. In order to accurately simulate the theoretical geometric structure of the GaSe/SnS_2 ($SnSe_2$) vdWHs, the freestanding GaSe and SnS_2 ($SnSe_2$) should be discussed. The optimized lattice constants are $a = b = 3.82$ Å for GaSe, $a = b = 3.70$ Å for the SnS_2 monolayer, and $a = b = 3.88$ Å for the $SnSe_2$ monolayer, which are consistent with previous publications [57–59]. This indicates that the lattice mismatch rate of the GaSe/SnX_2 (X = S, Se) vdWHs is far less than that of the GaSe and MoS_2 ($a = 3.18$ Å), $MoSe_2$ ($a = 3.28$ Å), WS_2 ($a = 3.19$ Å), and WSe_2 ($a = 3.34$ Å) heterojunctions [57,60].

A 1×1 GaSe monolayer and 1×1 SnS_2 ($SnSe_2$) monolayer are applied to construct the GaSe/SnS_2 ($SnSe_2$) vdWHs via the ATOMISTIX TOOLKIT software package [61].

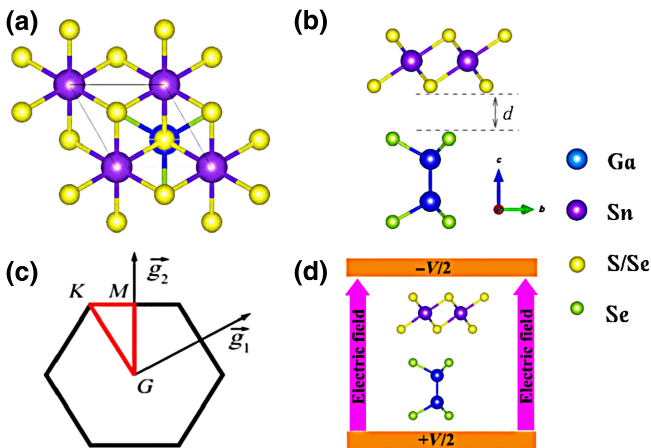

FIG. 1. (a) Top view and (b) side view of the relaxed geometric structure of GaSe/SnS_2 ($SnSe_2$) vdWHs. (c) The first Brillouin zone of the hexagonal monolayer with the vectors in the reciprocal lattice, high-symmetry points, and integral path. (d) Schematic model of the GaSe/SnS_2 ($SnSe_2$) vdWHs in the electric field.

The average lattice mismatch rate along the x and y directions is 1.06% (0.52%), both less than 5%, which is considered reasonable in the calculation. This can be attributed to the rhomboid structures of the 2D GaSe monolayer, SnS_2 monolayer, and $SnSe_2$ monolayer, resulting in a smaller lattice mismatch rate in the construction of the heterojunction. In addition, in order to further verify the influence of the strain generated by the lattice mismatch on the electronic structure of a single cell, we draw the band structure of each component in the heterojunction with and without the strain induced by the lattice mismatch [61]. Figure S2 in the Supplemental Material [61] shows that there are no significant changes in the band gap and the band trend. Therefore, the strain has no obvious effect on the electronic properties of the GaSe, SnS_2, and $SnSe_2$ monolayers.

Furthermore, we systematically consider the selection of the interlayer distance and the heterojunction binding energy for the construction of the GaSe/SnS_2 ($SnSe_2$) vdWHs. The binding energy is calculated using the following formula:

$$E_b = E_{\mathrm{GaSe/SnS_2(SnSe_2)}} - E_{\mathrm{GaSe}} - E_{\mathrm{SnS_2(SnSe_2)}} \qquad (1)$$

where $E_{\mathrm{GaSe/SnS_2(SnSe_2)}}$, E_{GaSe}, and $E_{\mathrm{SnS_2(SnSe_2)}}$ represent the total energies of the vdWHs, isolated GaSe, and isolated SnS_2 ($SnSe_2$) monolayers, respectively. The binding energy (E_b) corresponding to the GaSe/SnS_2 and GaSe/$SnSe_2$ vdWHs is taken as a function of the interlayer distances d_1 and d_2, as shown in Fig. S3 [61]. The results show that the optimal interlayer spacing of both GaSe/SnS_2 and GaSe/$SnSe_2$ vdWHs is 3.1 Å. This is much larger than the sum of the covalent radii between the Se and S (Se) atoms, indicating the existence of a weak vdW interaction between the two layers of the heterojunction. In addition, the corresponding negative value of the binding energies is a minimum, indicating that the two vdWHs are energetically stable.

In order to explore the formation mechanism and the application prospects of the GaSe/SnS_2 ($SnSe_2$) vdWHs, we study the electronic structures of each component and their vdWHs. Figure 1(c) plots the first Brillouin region of a hexagonal single-layer structure whose vectors are in the reciprocal lattice, the high-symmetry points, and the integral path. The GaSe, SnS_2, and $SnSe_2$ monolayers are all hexagonal lattices with similar lattice parameters, so their reciprocal lattice lengths are similar. The energy band structures of the GaSe, SnS_2, $SnSe_2$ monolayers, and vdWHs calculated with the PBE (HSE06) method are shown in Fig. 2. The red and blue (green) dots represent the weights of the GaSe and SnS_2 ($SnSe_2$). All of the band structures exhibit indirect band gaps. The conduction band minimum (CBM) is located at the G point, and the valence band maximum (VBM) is located on the G-K path. The PBE (HSE06) method is used to calculate the band gaps of 1.72 eV (2.65 eV) for the isolated GaSe monolayer, 1.6 eV

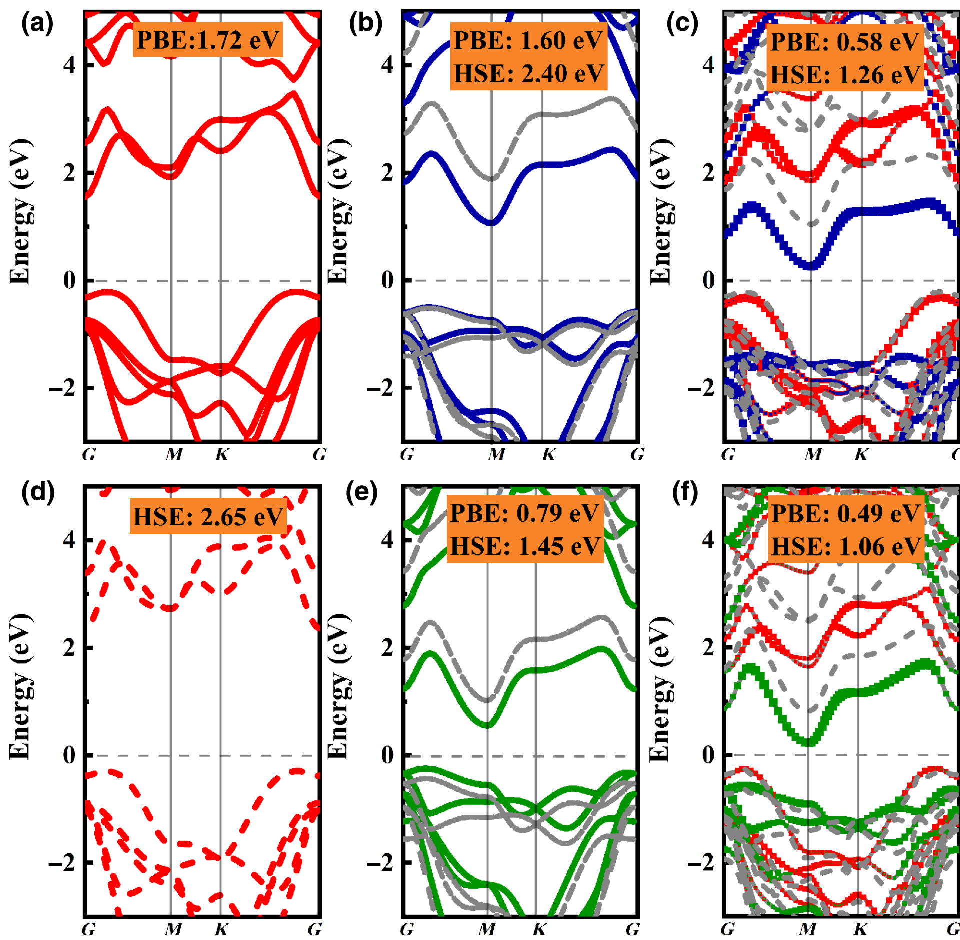

FIG. 2. The electronic structures of (a) and (d) 1×1 GaSe monolayer, and (b) and (e) 1×1 SnS_2 ($SnSe_2$) monolayer, and the calculated electronic band structure for (c) GaSe/SnS_2 vdWHs and (f) GaSe/$SnSe_2$ vdWHs. The solid (dashed) line indicates the PBE (HSE06) method, and the horizontal dashed line indicates the Fermi level. The Fermi level is set at zero.

(2.4 eV) for the isolated SnS_2, and 0.79 eV (1.45 eV) for the $SnSe_2$ monolayer. This is very consistent with the previously published band gap values of 1.6 eV (2.40 eV) for SnS_2 and 0.76 eV (1.36 eV) for $SnSe_2$ [59,61–63]. In addition, the band gap of the GaSe/SnS_2 vdWHs in the equilibrium state of approximately 0.58 eV (1.26 eV) and the band gap of the GaSe/$SnSe_2$ vdWHs of approximately 0.49 eV (1.06 eV) for the PBE (HSE06) method are obviously smaller than that of the monolayer, which indicates that the generated electrons are more likely to transfer from the valence band (VB) to the conduction band (CB) after the vdWHs are excited by light. Compared with the HSE06 method, the PBE method can obtain almost the same theoretical band trend more conveniently. Therefore, we use the PBE method to study and explore the changing trend of the electronic properties of the GaSe/SnX_2 ($X = $S, Se) under the action of a continuously changing external electric field, which has a certain guiding role for future experimental research.

By comparing Figs. 2(a)–2(f), it can be observed that the electronic properties of the GaSe monolayer and the SnS_2 ($SnSe_2$) monolayer are well preserved in the combination. This can be attributed to the weak vdW interaction between the GaSe and SnS_2 ($SnSe_2$) layers in the vdWHs and the small effect of the strain caused by the lattice mismatch. In addition, the CBM of the vdWHs located at the *G* point is provided by the single-layer SnS_2 ($SnSe_2$), while the CBM located on the *G*-*K* path is provided by the single-layer GaSe. More interestingly, the CBM and the VBM of the SnS_2 ($SnSe_2$) layer are lower in energy than the corresponding band edges of the GaSe layer, forming the crossover arrangement of the type-II bands, which promotes the separation of free electrons and hole spaces. Table S1 in the Supplemental Material [61] details the various structural properties of the GaSe/SnX_2 ($X = $S, Se) vdWHs. In order to intuitively show the characteristics of the band alignment further, the band alignment and the projected band structures of the GaSe/SnS_2 and the GaSe/$SnSe_2$ vdWHs are also drawn in Figs. 3(a) and 3(b).

B. Formation mechanism of type-II GaSe/SnS_2 ($SnSe_2$) vdWHs

Figures 3(a) and 3(b) show the band arrangement and the band structure projection schematic of the GaSe/SnS_2 and GaSe/$SnSe_2$ vdWHs. The vacuum energy level is used as the common energy reference. The E_g and E_F represent the energies of the band gap and the Fermi levels. The conduction band offset (CBO) and valence band offset (VBO) represent the band steps at the bottom of the conduction

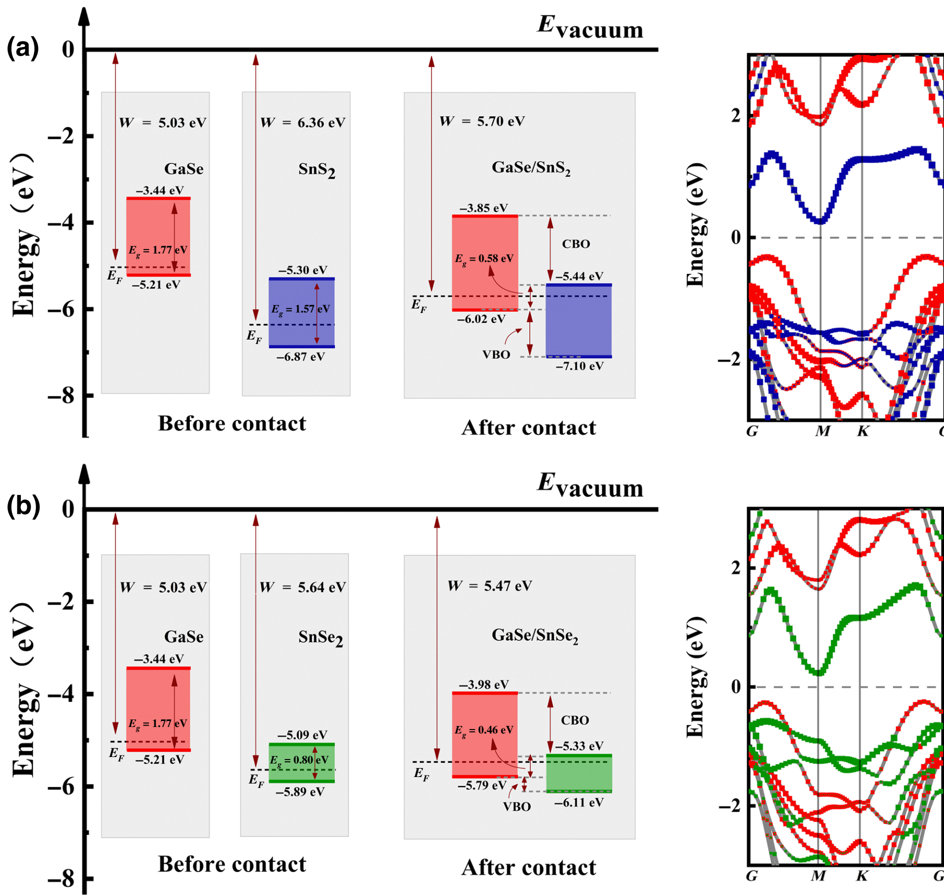

FIG. 3. The schematic diagram of the band alignment and the projected band structures of the (a) $GaSe/SnS_2$ and (b) $GaSe/SnSe_2$ vdWHs using the PBE method, using a vacuum level as a common energy reference. E_g and E_F represent the energy of the band gap and the Fermi level. The conduction band offset (CBO) and the valence band offset (VBO) represent the band steps at the bottom of the conduction band and the top of the valence band of the two substances, respectively.

band and at the top of the valence band of the two substances, respectively. The work function is defined as the difference between the electrostatic potential in the vacuum region and the Fermi level

$$\Delta\Phi = E_{\text{vacuum}} - E_F \tag{2}$$

where E_{vacuum} is the vacuum energy level of a stationary electron, and E_F represents the Fermi level of the corresponding system. The Fig. S4 [61] shows that the work function of the GaSe is calculated to be 5.03 eV, while the work function is calculated to be 6.36 and 5.64 eV for the SnS_2 and $SnSe_2$ monolayers, respectively. Compared with the GaSe monolayer, the work functions of the SnS_2 and $SnSe_2$ monolayers are higher. When the $GaSe/SnS_2$ ($SnSe_2$) vdWHs are formed, the charges tend to transfer from GaSe to the SnS_2 ($SnSe_2$) monolayer, resulting in the accumulation of negative charge in the SnS_2 ($SnSe_2$) layer and positive charge in the GaSe layer. Thus, there is a built-in electric field from the GaSe layer to the SnS_2 ($SnSe_2$) layer. In addition, the accumulated electrons in the SnS_2 ($SnSe_2$) layer cause the edge of the conduction band to drop owing to the electron occupation in the conduction band.

Moreover, it can be seen from Fig. 3 that the CBM and the VBM of the GaSe layer are higher than those of the SnS_2 ($SnSe_2$) layer. The CBO is 1.59 eV (1.35 eV) and the VBO is 1.08 eV (0.31 eV), which are typical characteristics of type-II vdWHs. The type-II heterojunction facilitates electron transfer from one component to another, which improves the separation efficiency of the electron-hole pairs at the interface of the heterostructures. In other words, the GaSe and SnX_2 ($X = $S, Se) act as electron donors and electron acceptors, respectively. This is very consistent with the results of the band structures discussed.

To further understand the spatial charge redistribution and the charge transfer between the GaSe and SnS_2 ($SnSe_2$) monolayers in the vdWHs, the three-dimensional charge density difference diagrams and the planar average charge density difference are obtained, as shown in Fig. 4. The charge density difference can be calculated as

$$\Delta\rho = \rho_{\text{vdWH}} - \rho_{\text{GaSe}} - \rho_{\text{SnS}_2(\text{SnSe}_2)} \tag{3}$$

where ρ_{vdWH} represents the charge density of the $GaSe/SnS_2$ or $GaSe/SnSe_2$ vdWHs, and ρ_{GaSe} and $\rho_{\text{SnS}_2(\text{SnSe}_2)}$ represent the charge densities of the isolated GaSe and SnS_2 ($SnSe_2$) monolayers in the same configuration, respectively. Figures 4(a) and 4(b) show the three-dimensional charge density difference plots along the z direction of the (a) $GaSe/SnS_2$ and (b) $GaSe/SnSe_2$

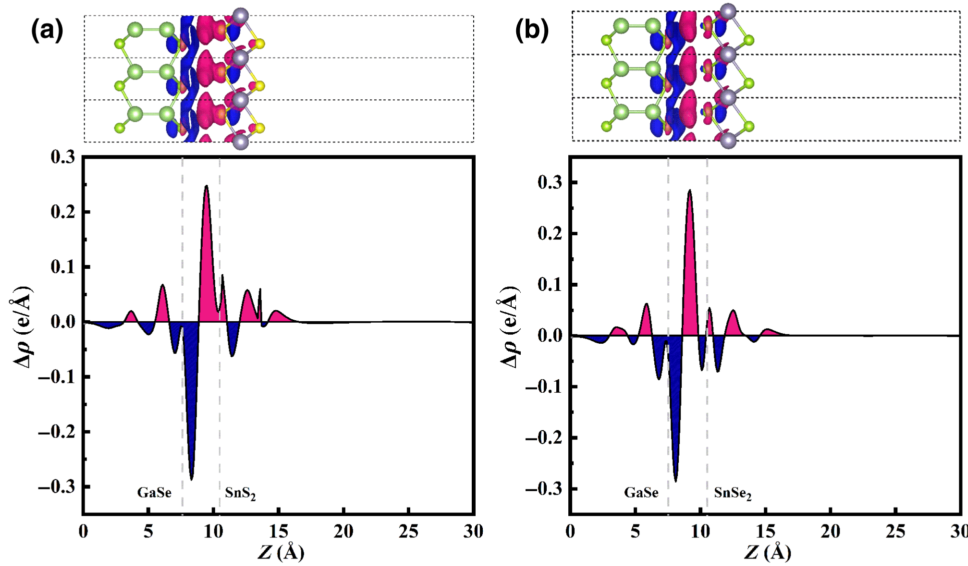

FIG. 4. Lateral views of the three-dimensional charge density difference diagrams and the planar average charge density difference $\Delta\rho(z)$ along the z direction of (a) $GaSe/SnS_2$ and (b) $GaSe/SnSe_2$ vdWHs. The area of $\Delta\rho > 0$ with a red and $\Delta\rho < 0$ with a blue isosurface represent the charge accumulation and depletion.

vdWHs and the side views of the plane mean charge density difference $\Delta\rho(z)$. The red region $\Delta\rho > 0$ and the blue region $\Delta\rho < 0$ indicate the accumulation and depletion of charge, respectively. The oscillation curves indicate that interlayer charge transfer occurs between monomers, and the amplitude of oscillation increases significantly near the interface. The results show that the charge is concentrated in the vicinity of the SnS_2 ($SnSe_2$) layer and depleted in the vicinity of the GaSe layer. In other words, the charge can be transferred from the GaSe layer to the SnS_2 ($SnSe_2$) layer in the heterostructures, resulting in the separation of electron-hole pairs.

C. Electric-field-tunable band alignments of $GaSe/SnS_2$ ($SnSe_2$) vdWHs

In practical applications, the gate voltage plays an important role in regulating the electronic performance of semiconductor devices. Therefore, we are particularly curious about what interesting effects the external electric field may have on $GaSe/SnS_2$ ($SnSe_2$) vdWHs. The schematic model of an electric field is shown in Fig. 1(d). The electronic band structures of $GaSe/SnX_2$ ($X =$ S, Se) vdWHs are researched in an external electric field applied along the z direction, which points from the GaSe layer toward the SnX_2 layer. It should be noted that the direction of the positive electric field is the same as the direction of the built-in electric field. The projected band structures and the corresponding band arrangements of $GaSe/SnS_2$($SnSe_2$) vdWHs for several selected electric fields are shown in Figs. 5 and 6. Additionally, Figs. S5 and S6 in the Supplemental Material [61] display detailed drawings of the projected band structure of $GaSe/SnS_2$ ($SnSe_2$) vdWH in different electric fields using 0.05 V/Å as a unit.

The calculated results show that the band gaps of $GaSe/SnS_2$ vdWHs gradually increase as the electric field changes from -0.4 to 0.4 V/Å, and the three band arrangements appear in turn. With the increase of the positive electric field, the type-II band alignment of the $GaSe/SnS_2$ heterojunction gradually changes into the type-I band alignment. The type-II heterostructures are characterized by the CBM and VBM provided by different materials. The type-I heterostructures can be used for luminescent applications with the features of CBM and VBM located in the same material. In other words, the CBM and the VBM of $GaSe/SnS_2$ vdWHs are provided by the VBM of SnS_2 and the VBM of GaSe, respectively, and they gradually change to both be contributed by the SnS_2 layer. In this case, both electrons and holes can be transferred to the SnS_2 layer, inducing a rapid recombination of electrons and holes, which can be used in LEDs. When a strong enough negative electric field $E = -0.2$ V/Å is applied, the projected band structure exhibits type-III band alignment, allowing charges to directly tunnel from the VBM of the GaSe to the CBM of the SnS_2, turning on the TFETs with a band-to-band tunneling (BTBT) transport mechanism. As the negative electric field intensity increases, the tunneling window is further widened with the increase of the tunneling probability and the tunneling current. In different electric fields, the $GaSe/SnSe_2$ vdWHs also show similar behavior. When the electric field applied to the $GaSe/SnS_2$ vdWHs is varied from -0.2 to 0.2 V/Å, the variable band gap and three kinds of band alignments, type-III, type-II, and type-I, appear in turn. The type-II band alignment means that the electrons tend to transfer to the $SnSe_2$ layer, and that the holes are often located in the GaSe layer, which promotes the efficient separation of electrons and holes, prolongs the life of excitons, and allows the applications of heterostructures in high-performance photovoltaic devices and the photocatalytic decomposition of water. In addition, with the increase of the negative electric field, the type-III

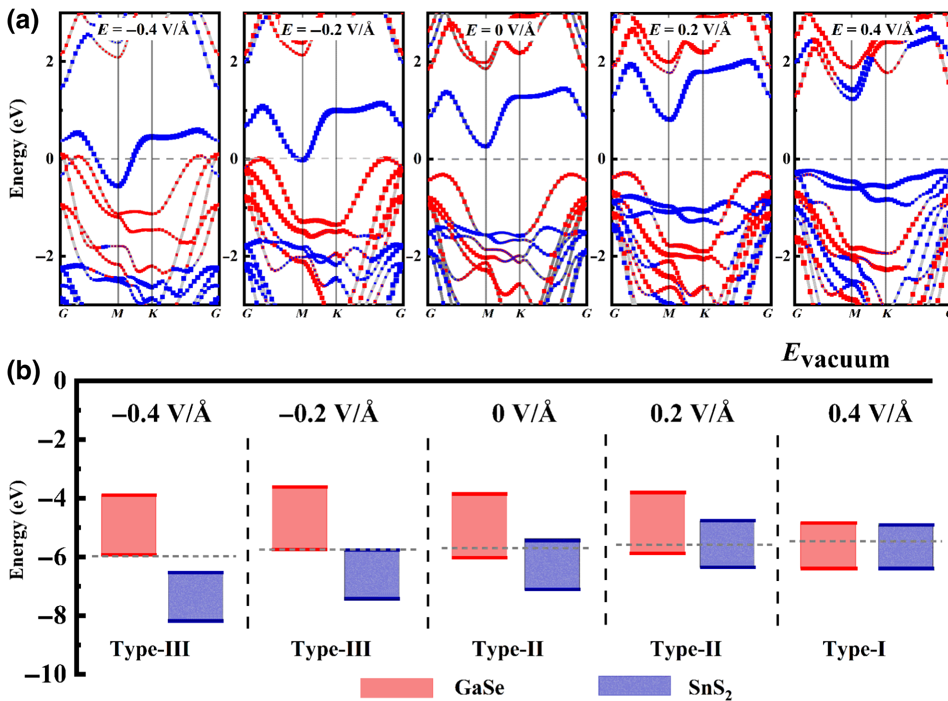

FIG. 5. The (a) projected band structures and (b) corresponding band alignments in external electric fields of −0.4, −0.2, 0, 0.2, and 0.4 V/Å for $GaSe/SnS_2$ vdWHs. The red and blue lines represent the GaSe and SnS_2 layers, respectively. The Fermi level is set to zero.

band alignment can be obtained, resulting in the charge directly tunneling from the VBM of the GaSe to the CBM of the $SnSe_2$. Thus, a tunneling window is formed when the VBM of the GaSe is located higher than the CBM of the $SnSe_2$, turning on the heterojunction-based devices.

In order to study the interesting situation of $GaSe/SnS_2$ ($SnSe_2$) vdWHs in different electric fields intuitively and simply, the curves of the band gap and the band edge as a function of the electric fields in $GaSe/SnS_2$ and $GaSe/SnSe_2$ are designed as shown in Fig. 7. As can be seen from Fig. 7(a), when the positive electric field increases from 0 to 0.39 V/Å, the band gap of the $GaSe/SnS_2$ increases almost linearly from 0.58 to 1.47 eV, and when the negative electric field increases from 0 to 0.2 V/Å, the band gap decreases almost linearly from 0.58 to 0 eV. For the $GaSe/SnSe_2$ vdWHs, as shown in Fig. 7(b), when the positive electric field increases

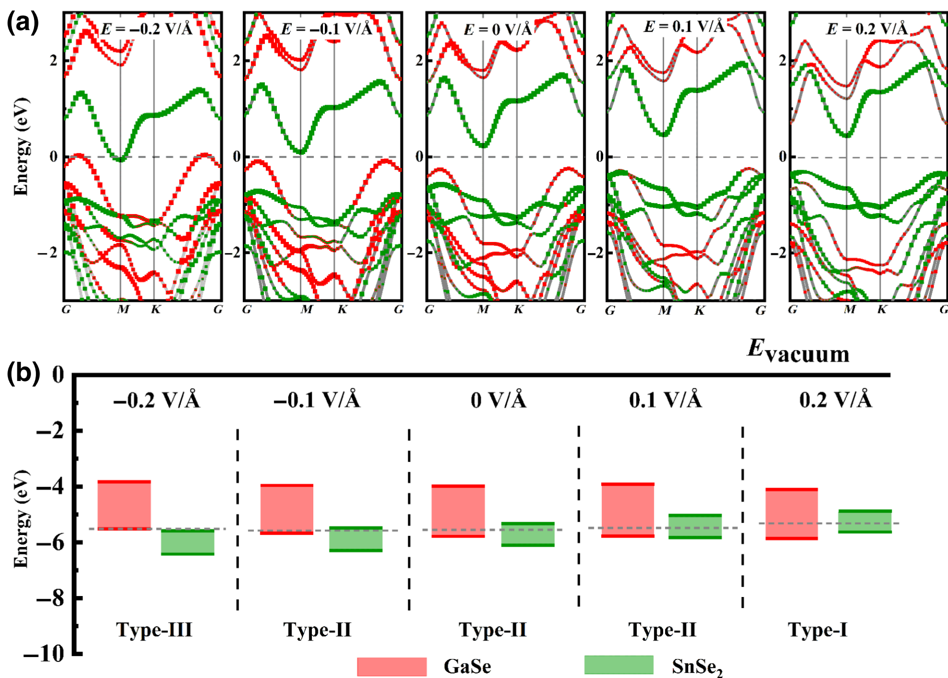

FIG. 6. The (a) projected band structures and (b) corresponding band alignments in external electric fields of −0.2, −0.1, 0, 0.1, and 0.2 V/Å for $GaSe/SnSe_2$ vdWHs. The red and green lines represent the GaSe and $SnSe_2$ layers, respectively. The Fermi level is set to zero.

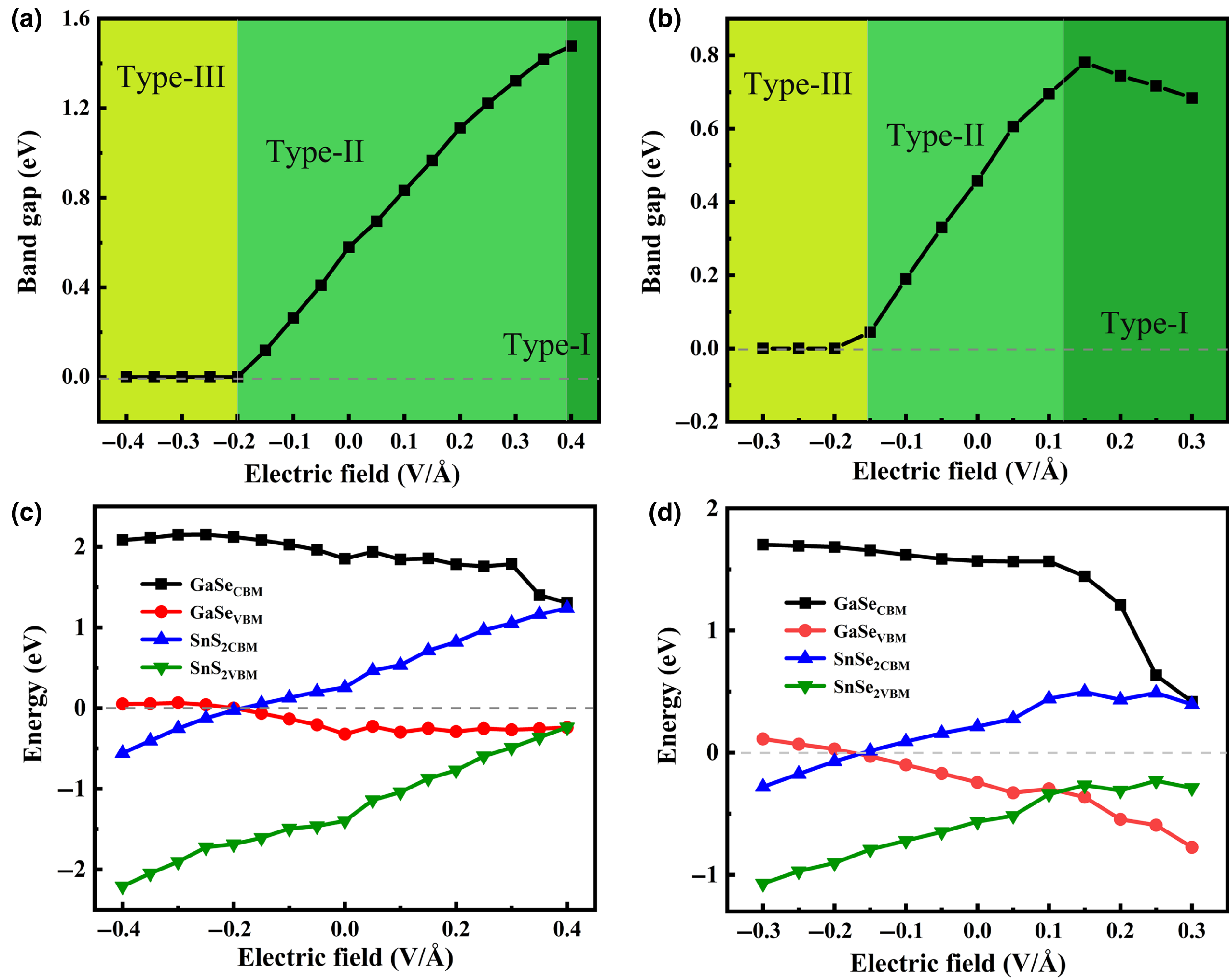

FIG. 7. The evolution of the band gap and the band edge as a function of the electric field in the (a) and (c) GaSe/SnS$_2$ and (b) and (d) GaSe/SnSe$_2$ vdWHs. The black, red, blue, and green lines represent the CBM of the GaSe, the VBM of the GaSe, the CBM of the SnS$_2$ (SnSe$_2$), and the VBM of the SnSe$_2$ (SnSe$_2$), respectively.

from 0 eV, the band gap first increases, then reaches the maximum value of 0.78 eV at 0.15 V/Å, and then decreases. When an increasing negative external field is applied, the band gap is almost linearly reduced to 0 eV, and the properties of the heterojunction are changed from a semiconductor to a metal. In other words, the GaSe/SnS$_2$ heterojunction can produce the transition from type-II to type-III in an electric field close to -0.2 V/Å, and from type-II to type-I in an electric field close to 0.39 V/Å. The other heterojunction, GaSe/SnSe$_2$, has a transition voltage critical point of about -0.16 V/Å from type-II to type-III and a transition voltage critical point of about 0.12 V/Å from type-II to type-I. In practical applications, compared with the GaSe/SnS$_2$ vdWHs, GaSe/SnSe$_2$ vdWHs can more easily and flexibly complete the regulation of band alignment between types-I, -II, and -III. Figures 7(c) and 7(d) show the band edges of the GaSe and SnS$_2$ (SnSe$_2$) layers, the constituent parts of the GaSe/SnX_2 ($X =$ S, Se) heterojunction, relative to their Fermi levels. The results show that with the increase of the negative field, the decrease of the CBM of the SnS$_2$ (SnSe$_2$), and the increase of the VBM of the GaSe are the direct cause of the transformation of the system to type-III. With the action of a positive electric field, the increase of the VBM in the SnS$_2$ (SnSe$_2$) monolayer and the decrease of the VBM in the GaSe can lead to the type-I band alignment of the vdWHs. All these findings suggest that the electric field can effectively regulate the electronic properties, including the band edge position, band gap, and band alignment of the GaSe/SnS$_2$ (SnSe$_2$), which will be used to fabricate high-performance nanodevices in the near future.

D. Response of GaSe/SnS$_2$ (SnSe$_2$) vdWHs to external electric field under different lattice strains

In addition, we study the electronic structures of the GaSe/SnS$_2$ (SnSe$_2$) vdWHs with different lattice

TABLE I. The band gap (E_g) of the GaSe and SnS_2 obtained for $2\sqrt{3} \times \sqrt{13}$ and 1×1 supercells with the different lattice constants a.

	GaSe-SnS_2 vdWHs			GaSe	SnS_2
System a (Å)	E_g (eV)	Turning points (II-III) (V/Å)	Turning points (II-I) (V/Å)	E_g (eV)	E_g (eV)
13.2	0.51	−0.17	0.35	1.74	1.53
3.70	0.70	−0.22	0.33	2.47	1.59
3.72	0.66	−0.22	0.35	2.34	1.60
3.74	0.62	−0.21	0.40	2.22	1.60
3.76	0.58	−0.20	0.39	2.10	1.61
3.78	0.56	−0.19	0.40	1.98	1.62
3.80	0.52	−0.19	0.39	1.87	1.63

The band gap (E_g) of the GaSe/SnS_2 vdWHs with the different lattice constants (a), and the turning points from type-II to type-III and from type-II to type-I under the electric field. The optimized lattice constant of the GaSe/SnS_2 vdWHs is $a = b = 13.2$ Å.

constants, and explore the responses of vdWHs with different strain to electric field adjustment. The band gap of the GaSe/SnS_2 ($SnSe_2$) vdWHs with the different lattice constants, and the turning points from type-II to type-III and from type-II to type-I under the electric field are shown in Tables I and II. The detailed information and results on the $2\sqrt{3} \times \sqrt{13}$ GaSe/SnS_2 vdWHs are shown in the Supplemental Material [61]. As shown in Table I, with the increase in lattice constant from 3.70 to 3.80 Å, the band gap of GaSe/SnS_2 vdWHs decreases from 0.70 to 0.52 eV. The band gap decreases from 2.47 to 1.87 eV for GaSe and increases from 1.59 to 1.63 eV for SnS_2. Meanwhile, the GaSe/SnS_2 vdWHs with different lattice constants have similar responses to an electric field. The transition from type-II to type-I occurs in a positive electric field and from type-II to type-III occurs in a negative electric field. It should be pointed that the turning points from type-II to type-I in the GaSe/$SnSe_2$ vdWHs with the different lattice constants are between 0.33 and 0.40 V/Å, while the turning points from type-II to type-III are between −0.19 and −0.22 V/Å.

It can be seen in Table II that similar results are found in the GaSe/$SnSe_2$ vdWHs. With the increase in lattice constant from 3.82 to 3.88 Å, the band gap of GaSe/$SnSe_2$ vdWHs decreases from 0.52 to 0.43 eV. The band gap decreases from 2.47 to 1.87 eV for GaSe and varies between 0.74 and 0.80 eV for $SnSe_2$. When positive and negative electric fields are applied to the GaSe/$SnSe_2$ vdWHs with different lattice constants, the transition from type-II to type-III or type-I can be generated, respectively. The turning points from type-II to type-I are between 0.1 and 0.12 V/Å, and the turning points from type-II to type-III are within the effective range of −0.16 to −0.18 V/Å.

TABLE II. The band gap (E_g) of the GaSe and $SnSe_2$ obtained for 1×1 supercells with the different lattice constants a.

	GaSe-$SnSe_2$ vdWHs			GaSe	$SnSe_2$
System a (Å)	E_g (eV)	Turning points (II-III) (V/Å)	Turning points (II-I) (V/Å)	E_g (eV)	E_g (eV)
3.82	0.52	−0.18	0.10	1.73	0.74
3.84	0.49	−0.18	0.11	1.63	0.76
3.86	0.48	−0.17	0.10	1.58	0.75
3.88	0.43	−0.16	0.12	1.53	0.80

The band gap (E_g) of the GaSe/$SnSe_2$ vdWHs with the different lattice constants (a), and the turning points from type-II to type-III and from type-II to type-I under the electric field.

To sum up, the band gap and electric field turning points will change due to the influence of the strain. However, the GaSe/SnS_2 ($SnSe_2$) vdWHs have similar responses to the electric field. In a specific positive electric field, the transition of band alignment from type-II to type-I occurs, and in a specific negative electric field, the transition from type-II to type-III occurs.

IV. CONCLUSION

In summary, our work demonstrates theoretically through DFT calculations that a vertical electric field can effectively, flexibly, and dynamically regulate the band structure and electronic properties of type-II GaSe/SnX_2 ($X =$ S, Se) vdWHs, making it a good candidate material for photodetector and field-effect transistor applications. A positive electric field can control the band alignment transformation from type-II to type-I with electric field values of about 0.39 V/Å (0.13 V/Å), while a negative electric field can transform the type-II to type-III band alignments with electric field values of about −0.18 V/Å (−0.16 V/Å) in the GaSe/SnS_2 ($SnSe_2$) vdWHs. We trace these surprising results to the conduction band and valence band edge position movements for the linear decrease of the GaSe, as well as the linear increase of the SnS_2 ($SnSe_2$) with the applied electric field. For the electric field regulation, our designed GaSe-SnX_2 ($X =$ S, Se) heterojunctions can complete the band-type regulation between type-I, type-II, and type-III within a range of about 0.4 V/Å, or even 0.12 V/Å, so GaSe-SnX_2 ($X =$ S, Se) heterojunctions can be flexibly regulated. Moreover, type-I vdWHs are suitable for LEDs, type-II vdWHs for light capture in the photovoltaics field, and type-III vdWHs for TFETs. In addition, since a heterojunction is inevitably affected by an applied electric field, the theoretical results of this study can be used to predict the response of a heterojunction in different electric fields. Therefore, the present work provides a direction for the development of tunable multiband

alignment technology in 2D vdWHs and the application of multifunctional devices.

ACKNOWLEDGMENTS

The authors thank the Changsha Supercomputer Center for computation. This work is supported by the National Natural Science Foundation of China (Grants No. 51972103 and No. 21938002). This project is supported by the open foundation of Guangxi Key Laboratory of Processing for Non-ferrous Metals and Featured Materials, Guangxi University (Grant No. 2021GXYSOF) and Guangxi Natural Science Foundation (Grant No. 2017GXNSFGA198005).

[1] W. Choi, N. Choudhary, G. H. Han, J. Park, D. Akinwande, and Y. H. Lee, Recent development of two-dimensional transition metal dichalcogenides and their applications, Mater. Today **20**, 116 (2007).

[2] C. S. Liao, Z. L. Yu, P. B. He, Y. Q. Zhao, B. Liu, and M. Q. Cai, Theoretical study on the tunable electronic band structure of $Cs_2PbI_2Cl_2/CsPbBr_3$ halide perovskite heterostructure driven by ferroelectric polarization modulation, J. Power. Sources **478**, 229078 (2020).

[3] Q. H. Li, Y. F. Ding, P. B. He, R. S. Zeng, Q. Wan, and M. Q. Cai, Transition of the type of band alignments for all-inorganic perovskite van der Waals Heterostructures $CsSnBr_3/WS_{2(1-x)}Se_{2x}$, J. Phys. Chem. Lett. **12**, 3809 (2021).

[4] C. S. Liao, Z. L. Yu, P. B. He, B. Liu, R. S. Zeng, Q. Wan, and M. Q. Cai, Effects of composition modulation on the type of band alignments for $Pd_2Se_3/CsSnBr_3$ van der waals heterostructure: A transition from type I to type II, J. Colloid Interf. Sci. **597**, 233 (2021).

[5] K. S. Novoselov, A. K. Geim, S. V. Morozov, D. Jiang, M. I. Katsnelson, I. V. Grigorieva, S. V. Dubonos, and A. A. Firsov, Two-dimensional gas of massless Dirac fermions in graphene, Nature **438**, 197 (2005).

[6] J. R. Zhang, X. Z. Deng, B. Gao, L. Chen, C. T. Au, K. L. Li, S. F. Yin, and M. Q. Cai, Theoretical study on the intrinsic properties of In_2Se_3/MoS_2 as a photocatalyst driven by near-infrared, visible and ultraviolet light, Catal. Sci. Technol. **9**, 4659 (2019).

[7] F. Schwierz, Graphene transistors, Nat. Nanotechnol. **5**, 487 (2010).

[8] Z. Z. Li, X. C. Meng, and Z. S. Zhang, Recent development on MoS_2-based photocatalysis: A review, J, Photochem. Photobiol. **35**, 39 (2018).

[9] F. Ceballos, M. Z. Bellus, H.-Y. Chiu, and H. Zhao, Ultrafast charge separation and indirect exciton formation in a MoS_2–$MoSe_2$ van der Waals Heterostructure, ACS Nano **8**, 12717 (2014).

[10] D. Jariwala, T. J. Marks, and M. C. Hersam, Mixed-dimensional van der Waals heterostructures, Nat. Mater. **16**, 170 (2017).

[11] J. E. Padilha, A. Fazzio, and A. J. R. da Silva, Van der Waals Heterostructure of Phosphorene and Graphene: Tuning the Schottky Barrier and Doping by Electrostatic Gating, Phys. Rev. Lett. **114**, 066803 (2015).

[12] Z. L. Yu, Y. Q. Zhao, B. Liu, and M. Q. Cai, Breaking the anisotropy of alpha-CNH and improving the photoelectric performance by constructing Van der Waals heterojunction, Appl. Surf. Sci. **497**, 143787 (2020).

[13] Z. L. Yu, Y. Q. Zhao, Q. Wan, B. Liu, J. L. Yang, and M. Q. Cai, Exploring the coexistence mechanism of $CsPb_2Br_5$ and $CsPbBr_3$ based on the competitive phase diagram, J. Phys. Chem. C **124**, 23052 (2020).

[14] T. Akamatsu, T. Ideue, L. Zhou, Y. Dong, S. Kitamura, M. Yoshii, D. Yang, M. Onga, Y. Nakagawa, K. Watanabe, T. Taniguchi, J. Laurienzo, J. Huang, Z. Ye, T. Morimoto, H. Yuan, and Yoshihiro Iwasa, A van der Waals interface that creates in-plane polarization and a spontaneous photovoltaic effect, Science **372**, 68 (2021).

[15] J. Miao, Z. Xu, Q. Li, A. Bowman, S. Zhang, W. Hu, Z. Zhou, and C. Wang, Vertically stacked and self-encapsulated van der Waals heterojunction diodes using two-dimensional layered semiconductors, ACS Nano **11**, 10472 (2017).

[16] E. Torun, H. P. C. Miranda, A. Molina-Sánchez, and L. Wirtz, Interlayer and intralayer excitons in MoS_2/WS_2 and $MoSe_2/WSe_2$ heterobilayers, Phys. Rev. B **97**, 245427 (2018).

[17] K. R. Williams, B. T. Diroll, N. E. Watkins, X. Rui, A. Brumberg, R. F. Klie, and R. D. Schaller, Synthesis of Type I PbSe/CdSe dot-on-plate heterostructures with near-infrared emission, J. Am. Chem. Soc. **141**, 5092 (2019).

[18] M. Z. Bellus, M. Li, S. D. Lane, F. Ceballos, Q. Cui, X. C. Zeng, and H. Zhao, Type-I van der Waals heterostructure formed by MoS_2 and ReS_2 monolayers, Nanoscale Horiz. **2**, 31 (2017).

[19] Y. Almadori, N. Bendiab, and B. Grévin, Multimodal kelvin probe force microscopy investigations of a photovoltaic WSe_2/MoS_2 Type-II interface, ACS Appl. Mater. Interfaces **10**, 1363 (2018).

[20] Y. Wang, Q. Wang, X. Zhan, F. Wang, M. Safdar, and J. He, Visible light driven type II heterostructures and their enhanced photocatalysis properties: A review, Nanoscale **5**, 8326 (2013).

[21] K. Datta and Q. D. M. Khosru, Simulation of thin-TFETs using transition metal dichalcogenides: Effect of material parameters, gate dielectric on electrostatic device performance, J. Comput. Electron. **16**, 228 (2017).

[22] R. Yan, S. Fathipour, Y. Han, B. Song, S. Xiao, M. Li, N. Ma, V. Protasenko, D. A. Muller, D. Jena, and H. G. Xing, Esaki diodes in van der Waals heterojunctions with broken-gap energy band alignment, Nano Lett. **15**, 5791 (2015).

[23] N. Shehzad, I. Shahid, S. Yao, S. Ahmad, A. Ali, L. Zhang, and Z. Zhou, A first-principles study of electronic structure and photocatalytic performance of two-dimensional van der Waals MTe_2–As (M = Mo, W) heterostructures, Int. J. Hydrog. Energy **45**, 27089 (2020).

[24] X. M. Jia, J. Cao, H. L. Lin, M. Y. Zhang, X. M. Guo, and S. F. Chen, Transforming type-I to type-II heterostructure photocatalyst via energy band engineering: A case study of I-BiOCl/I-BiOBr, Appl. Catal. B Environ. **204**, 505 (2017).

[25] X. Chen, Z.-Z. Lin, and M. Ju, Controllable band alignment transition in InSe − −MoS_2 Van der Waals heterostructure, Phys. Status Solidi RRL. **12**, 1800102 (2018).

[26] B. Zhou, K. Jiang, L. Shang, J. Zhang, Y. Li, L. Zhu, S. Gong, Z. Hu, and J. Chu, Enhanced carrier separation in ferroelectric In_2Se_3/MoS_2 van der Waals heterostructure, J. Mater. Chem. C **8**, 11160 (2020).

[27] K. Cheng, Y. Guo, N. Han, X. Jiang, J. Zhang, R. Ahuja, Y. Su, and J. Zhao, 2D lateral heterostructures of group-III monochalcogenide: Potential photovoltaic applications, *Appl. Phys. Lett*. **112**, 143902 (2018).

[28] H. Yang, P. Zhao, Y. Ma, X. Lv, B. Huang, and Y. Dai, Janus single-layer group-III monochalcogenides: A promising visible-light photocatalyst, *J. Phys. D: Appl. Phys*. **52**, 455303 (2019).

[29] M. Wasala, H. I. Sirikumara, Y. Raj Sapkota, S. Hofer, D. Mazumdar, T. Jayasekera, and S. Talapatra, Recent advances in investigations of the electronic and optoelectronic properties of group III, IV, and V selenide based binary layered compounds, J. Mater. Chem. C **5**, 11214 (2017).

[30] D. J. Late, B. Liu, J. Luo, A. Yan, H. S. S. R. Matte, M. Grayson, C. N. R. Rao, and V. P. Dravid, Gas and GaSe ultrathin layer transistors, *Adv. Mater*. **24**, 3549 (2012).

[31] X. Li, M.-W. Lin, A. A. Puretzky, J. C. Idrobo, C. Ma, M. Chi, M. Yoon, C. M. Rouleau, I. I. Kravchenko, D. B. Geohegan, and K. Xiao, Controlled vapor phase growth of single crystalline, Two-dimensional GaSe crystals with high photoresponse, *Sci. Rep*. **4**, 5497 (2014).

[32] R. Lu, J. Liu, H. Luo, V. Chikan, and J. Z. Wu, Graphene/GaSe-nanosheet hybrid: Towards high gain and fast photoresponse, *Sci. Rep*. **6**, 19161 (2016).

[33] P. Hu, Z. Wen, L. Wang, P. Tan, and K. Xiao, Synthesis of Few-layer GaSe nanosheets for high performance photodetectors, ACS Nano **6**, 5988 (2012).

[34] V. Augelli, C. Manfredotti, R. Murri, and L. Vasanelli, Hall-mobility anisotropy in GaSe, Phys. Rev. B **17**, 3221 (1978).

[35] Z. Ben Aziza, V. Zólyomi, H. Henck, D. Pierucci, M. G. Silly, J. Avila, S. J. Magorrian, J. Chaste, C. Chen, M. Yoon, K. Xiao, F. Sirotti, M. C. Asensio, E. Lhuillier, M. Eddrief, V. I. Fal'ko, and A. Ouerghi, Valence band inversion and spin-orbit effects in the electronic structure of monolayer GaSe, Phys. Rev. B **98**, 115405 (2018).

[36] P. E. Lippens, M. El Khalifi, and M. Womes, Electronic structures of SnS and SnS_2, Phys. Status Solidi B **254**, 1600194 (2017).

[37] J. Chao, Z. Xie, X. Duan, Y. Dong, Z. Wang, J. Xu, B. Liang, B. Shan, J. Ye, D. Chen, and G. Shen, Visible-light-driven photocatalytic and photoelectrochemical properties of porous SnSx(x = 1,2) architectures, CrystEngComm **14**, 3163 (2012).

[38] Y. Sun, H. Cheng, S. Gao, Z. Sun, Q. Liu, Q. Liu, F. Lei, T. Yao, J. He, S. Wei, and Y. Xie, Freestanding Tin disulfide single-layers realizing efficient visible-light water splitting, Angew. Chem. Int. Ed. **51**, 8727 (2012).

[39] N. Zhou, R. Wang, X. Zhou, H. Song, X. Xiong, Y. Ding, J. Lü, L. Gan, and T. Zhai, P-GaSe/N-MoS_2 vertical heterostructures synthesized by van der Waals epitaxy for photoresponse modulation, Small **14**, 1702731 (2018).

[40] P. Perumal, R. Kumar Ulaganathan, R. Sankar, and L. Zhu, Staggered band offset induced high performance opto-electronic devices: Atomically thin vertically stacked GaSe-SnS_2 van der Waals p-n heterostructures, Appl. Surf. Sci. **535**, 147480 (2021).

[41] G. Kresse and J. Hafner, Theory of the crystal structures of selenium and tellurium: The effect of generalized-gradient corrections to the local-density approximation, Phys. Rev. B **49**, 13181 (1994).

[42] D. N. Yan, C. S. Liao, Y. Q. Zhao, and M. Q. Cai, Theoretical prediction of double perovskite $Cs_2Ag_xCu_{1-x}In_yTb_{1-y}Cl_6$ for infrared detection, J. Phys. D: Appl. Phys. **53**, 265302 (2020).

[43] L. Y. Pan, F. F. Ding, Z. L. Yu, and M. Q. Cai, Layer-dependent optoelectronic property for all-inorganic two-dimensional mixed halide perovskite $Cs_2PbI_2Cl_2$ with a ruddlesden-popper structure, J. Power Sources **451**, 227732 (2020).

[44] M. Y. Qian, Z. L. Yu, Q. Wan, P. B. He, B. Liu, J. L. Yang, and M. Q. Cai, Effects of components modulation on the type of band alignments for PbI_2/WS_2 van der Waals heterostructure, Phys. Status Solidi-RRL **14**, 2000016 (2020).

[45] G. Kresse and J. Furthmüller, Efficient iterative schemes for ab initio total-energy calculations using a plane-wave basis set, Phys. Rev. B **54**, 11169 (1996).

[46] P. E. Blöchl, Projector augmented-wave method, Phys. Rev. B **50**, 17953 (1994).

[47] J. P. Perdew, K. Burke, and M. Ernzerhof, Generalized Gradient Approximation Made Simple, Phys. Rev. Lett. **77**, 3865 (1996).

[48] Y. F. Ding, Z. L. Yu, P. B. He, Q. Wan, B. Liu, J. L. Yang, and M. Q. Cai, High-performance Photodetector Based on $InSe/Cs_2XI_2Cl_2$ (X = Pb, Sn, and Ge) Heterostructures, Phys. Rev. Appl. **13**, 064053 (2020).

[49] Z. L. Yu, Y. Q. Zhao, B. Liu, J. L. Yang, and M. Q. Cai, Band alignment engineering: Ultrabroadband photodetection with SnX_2 (X = S, Se)/ZnS heterostructures, J. Phys.:Condens. Matter **32**, 115703 (2020).

[50] Z. L. Yu, Y. Q. Zhao, P. B. He, B. Liu, J. L. Yang, and M. Q. Cai, The influence of electrode for electroluminescence devices based on all-inorganic halide perovskite $CsPbBr_3$, J. Phys.:Condens. Matter **32**, 065002 (2020).

[51] X. Z. Deng, J. R. Zhang, Y. Q. Zhao, Z. L. Yu, J. L. Yang, and M. Q. Cai, The energy band engineering for the high-performance infrared photodetectors constructed by $CdTe/MoS_2$ heterojunction, J. Phys.:Condens. Matter. **32**, 065004 (2020).

[52] Z. L. Yu, Y. Q. Zhao, Q. Wan, B. Liu, J. L. Yang, and M. Q. Cai, Theoretical study on the effect of the optical properties and electronic structure for the Bi-doped $CsPbBr_3$, J. Phys.:Condens. Matter **32**, 205504 (2020).

[53] S. Grimme, J. Antony, S. Ehrlich, and H. Krieg, A consistent and accurate ab initio parametrization of density functional dispersion correction (DFT-D) for the 94 elements H-Pu, J. Chem. Phys. **132**, 154104 (2010).

[54] M. Brandbyge, J.-L. Mozos, P. Ordejón, J. Taylor, and K. Stokbro, Density-functional method for nonequilibrium electron transport, Phys. Rev. B **65**, 165401 (2002).

[55] J. Heyd, G. E. Scuseria, and M. Ernzerhof, Hybrid functionals based on a screened Coulomb potential, J. Chem. Phys. **118**, 18 (2003).

[56] A. D. Becke, Perspective: Fifty years of density-functional theory in chemical physics, J. Chem. Phys. **140**, 18A301 (2014).

[57] K. D. Pham, H. V. Phuc, N. N. Hieu, B. D. Hoi, and C. V. Nguyen, Electronic properties of $GaSe/MoS_2$ and $GaS/MoSe_2$ heterojunctions from first principles calculations, AIP Adv. **8**, 075207 (2018).

[58] H.-Y. Wu, K. Yang, Y. Si, W.-Q. Huang, W. Hu, and G.-F. Huang, Two-dimensional GaX/SnS_2 ($X = S$, Se) van der Waals heterostructures for photovoltaic application: Heteroatom doping strategy to boost power conversion efficiency, Phys. Status Solidi RRL **13**, 1800565 (2019).

[59] C. Xia, J. Du, M. Li, X. Li, X. Zhao, T. Wang, and J. Li, Effects of Electric Field on the Electronic Structures of Broken-gap Phosphorene/SnX_2 ($X = S$, Se) van der Waals Heterojunctions, Phys. Rev. Appl. **10**, 054064 (2018).

[60] B. Amin, T. P. Kaloni, and U. Schwingenschlogl, Strain engineering of WS_2, WSe_2, and WTe_2, RSC Adv. **4**, 34561 (2014).

[61] See Supplemental Material at http://link.aps.org/supplemental/10.1103/PhysRevApplied.16.044003 for additional details, including the heterostructure matching diagrams, the lattice constants, calculated binding energies, the work function, and the band structures.

[62] Q. Zhang, X. Li, T. Wang, Z. Geng, and C. Xia, Band structure engineering of SnS_2/polyphenylene van der waals heterostructure via interlayer distance and electric field, Phys. Chem. Chem. Phys **21**, 1521 (2019).

[63] M. R. Yan, Y. F. Ding, B. Liu, R. S. Zeng, Q. Wan, and M. Q. Cai, Effects of component on the photoelectric properties of two-dimensional van der Waals heterostructure $Cs2PbI_{2(1+x)}Cl_{2(1-x)}/Pd_2Se_3$ with ruddlesen-popper structure, J. Phys. D-Appl. Phys. **54**, 355110 (2021).

Correction: The math terms in the HTML version were processed incorrectly in the production process and have been rendered properly now.